EFDA–JET–PR(12)54

M. Rack, B. Sieglin, T. Eich, J. Pearson, Y. Liang, I. Balboa,
A. Wingen, S.J.P. Pamela, and JET EFDA contributors

Findings of pre-ELM Structures Through the Observation of Divertor Heat Load Patterns at JET

Findings of pre-ELM Structures Through the Observation of Divertor Heat Load Patterns at JET

M. Rack [1], B. Sieglin[2], T. Eich[2], J. Pearson[1], Y. Liang[1],I. Balboa[3], A. Wingen[4], S.J.P. Pamela[5], and JET EFDA contributors*

JET-EFDA, Culham Science Centre, OX14 3DB, Abingdon, UK

[1]Institute of Energy and Climate Research - Plasma Physics, Forschungszentrum Jülich GmbH, Association EURATOM-FZJ, Partner in the Trilateral Euregio Cluster, D-52425 Jülich, Germany
[2]Max-Planck-Institut für Plasmaphysik, EURATOM-Association, D-85748 Garching, Germany
[3]EURATOM-CCFE Fusion Association, Culham Science Centre, OX14 3DB, Abingdon, OXON, UK
[4]Oak Ridge National Laboratory, PO Box 2008, Oak Ridge, Tennessee 37831-6169, USA
[5]IIFS-PIIM. Aix Marseille Universite- CNRS, 13397 Marseille Cedex 20, France
** See annex of F. Romanelli et al, "Overview of JET Results", (24th IAEA Fusion Energy Conference, San Diego, USA (2012)).*

Preprint of Paper to be submitted for publication in
Physical Review Letters

ABSTRACT

Resonant magnetic perturbation (RMP) experiments at JET with the ITER-Like Wall have shown the formation of pre-ELM footprint structures appearing a few milliseconds before and propagating radially outwards until the major divertor heat load, caused by type-I edge localized modes (ELMs), occurs. The formation of the pre-ELM structures is accompanied by a drop in the electron temperature at the plasma edge. A comparison with a thermoelectric edge currents model results in qualitative agreement to the observations, whereas the dynamics can be understood based on RMP enhanced ballooning modes.

1. INTRODUCTION

The Edge Localized Modes (ELMs) which appear in High-Confinement Mode (H-mode) plasmas have been one of the major topics of fusion research since they where first discovered at ASDEX [1, 2]. These ELMs lead to fast periodic losses of heat and particles causing strong increases in the heat flux to the target plates. Non-controlled type-I ELMs could cause severe damage to the plasma facing components in large scale fusion devices, such as ITER [3], therefore a full understanding of ELMs is crucial. The ELMs have been studied from various directions, e.g. Magnetohydrodynamic (MHD) behaviour through magnetics, heat loads on the divertor targets, release of particles to the Scrape-Off Layer (SOL) and changes to the topology of the plasma edge. Although a lot of measurements and research has been done in this area, the dynamics of ELMs are still not fully understood.

One of the most promising techniques to control ELMs is the use of nonaxisymmetric magnetic perturbation fields [4{6], commonly applied as Resonant Magnetic Perturbations (RMPs). Fast infra-red thermography is used on ASDEX Upgrade [7], DIII-D [8] and JET [9] as the key diagnostic for the study of ELM heat loads on the divertor plates when RMPs are applied. Elsewhere, the MAST tokamak uses a fast visible light camera for the observation of topology changes in the near X-point region and lament studies [10, 11]. Through these techniques splitting of the strike-lines has been observed when RMPs are imposed in Low-Confinement Mode (L-mode) discharges on various machines [12–15].

A RMP ELM control experiment has been performed on JET with the new ITER-Like Wall, which contains a Beryllium main chamber and a Tungsten divertor [16]. The Error Field Correction Coils (EFCCs) [17] are used for the application of RMP fields to the plasma. The EFCCs can create a magnetic perturbation with a toroidal mode number of $n = 1$ and $n = 2$. During the last shut-down the power supplies of the EFCCs have been upgraded to provide a current of up to 6kA, twice as much as before [5]. For the studies of the divertor heat loads pattern the upgraded infra-red thermography system [18, 19] has been used. The quality of the thermography data is enhanced with the ITER-Like Wall as the deposition of carbon layer on the divertor is no longer an issue [20]. In these experiments an $n = 2$ RMP field at an EFCC current of 5kA (so 80kAt in 16 turns) has been applied.

The recent experiments have shown pre-ELM structures seen as a change in the divertor heat load pattern. A few milliseconds before a large amount of heat flux caused by the ELM reaches the

outer divertor plate, a footprint structure is formed near the original strike- line position. This grows radially outwards until the major ELM heat load appears on the divertor plate. The structure then vanishes after the ELM. The time-scale of this footprint pattern development is large compared to the usual time-scale of ELM crashes.

This letter discusses the observation of the pre-ELM structures. These are of importance and interest for the understanding of the dynamic processes during ELM events and their control mechanisms by RMPs. A possible mechanism that could lead to the formation and propagation of such pre-ELM structures is discussed.

2. EXPERIMENTAL OBSERVATION

In figure 1 a comparison of the divertor heat loads with and without applied RMP fields is shown. Both plots on the bottom shows the heat flux deposition on the outer divertor, tile 5. The white region marks the gap between two lamellas of the new ITER-Like Wall divertor. The change of the radial position of the strike-line between the non-RMP and RMP case is caused by the applied EFCC fields and the shaping control during the discharge. For the case without RMPs we observe standard type-I ELMs as reported many times before [9, 21]. The ELM crash leads to a strong increase of the heat flux to the position of the original strike-line. In addition an ELM comes with a radial burst of particles deposited along the divertor plate in radial outward direction. The period between two ELM crashes shows the increase of heat flux at the strike-line, but no further structures. In the case of the applied RMPs a pattern, marked by the red ellipses, appears during the phase before an ELM crash. These structures continue up to the major heat flux increase at the ELM crash.

Figure 2 shows two ELM periods during the RMP phase. After each ELM crash the heat flux to the divertor plates is strongly reduced. During that time the pedestal temperature and density recovers. In the presented measurement, about 5ms before the next ELM crash occurs, the heat load at the strike-line increases from about 4MWm^{-2} to 7MWm^{-2}. Slightly after the increase of the strike-line heat load the mentioned footprint structures are created. These pre-ELM footprint structures are seen as parallel lines in the time trace of the divertor heat load ($2.76\text{m} < R < 2.79\text{m}$). The position of these footprint structures is not constant in time, but moves radially outward. Most of the lines are created at a radial position of 2.76m, with a distance of about 4cm to the original strike-line. Their radial speed along the divertor target can be determined as approximately 20ms^{-1}. In the range of a millisecond before the major heat load appears the strike-line heat flux is reduced again. The pre-ELM structures continues until the major ELM heat flux reaches the divertor plate. Compared to typical ELMs at JET the heat load patterns of these ELMs shows a split nature where the main heat load is not only deposited at the original strike-line position, but as well comparable high heat fluxes can be observed at different radial positions. At the first increase of the heat load at the original strike-line (red line) the outer edge electron temperature drops simultaneously with the increased heat load and D_α emission in the inter-ELM phase. After the formation of the pre-ELM structure the edge electron temperature continues to increase as before until the pedestal crash

due to the ELM. The crash of the pedestal brings a strong edge temperature and density loss [22].

Comparing the D_α and Be II emission light from the outer divertor plate during this phase shows that the pre-ELM structures only cause an increase of the D_α emission. The Be II emission stays unaffected by the structures and increases only due to the major heat flux caused by the ELM crash, which indicates that lower energetic particles are emitted.

Below an EFCC current of 2.5kA no pre-ELM structures on the outer divertor target could be observed. A similar threshold behaviour was recently found on MAST [11] dealing with the effect of RMPs on the topology change in the near X-point region.

A difference was found for different values of q_{95}. Compared to the case presented in figure 2 ($q_{95} = 3.2$) the separation of the created structure to the original strike-line and its propagation speed was found to be half for discharges with a higher edge safety factor ($3.5 < q_{95} < 4.5$). Figure 3 shows the heat load pattern on the outer divertor. The applied RMP field is based on the same EFCC current and conguration as above. The propagating structures are created in a distance of less than 2cm to the original strike-line. Their propagation speed is about 7ms^{-1}. This behaviour with similar parameters was observed for various discharges with a edge safety factor between 3.5 and 4.5. No strong q_{95} dependence was found regarding distance to original strike-line position and propagation speed in this range.

3. DIFFERENCE TO RADIAL PROPAGATING ELM FILAMENTS

The ELM event can be described as a MHD mode in the plasma edge which becomes non- linearly unstable causing an explosion of particles from the plasma edge to the SOL [23]. ELMs are accompanied by laments which are created in the plasma edge region during their onset. These laments separate from the plasma when the ELM crash occurs and propagate radially outwards until they hit the first wall. The analysis of data of different sized tokamaks has shown that the ELM lament propagation speed is typically in the range of 0.5kms^{-1} to 2kms^{-1} [24]. A usual JET plasma has a radial distance to the first wall of about 10cm at the mid-plane. The time the ELM lament spends in the SOL before interacting with the wall and collapsing, is therefore in the range of microseconds. While the observed pre-ELM structures appear on a range of milliseconds, they cannot be explained by the much faster radially propagating ELM laments. The same argumentation applies for inter-ELM laments that where found at MAST [25] to have a radial propagation speed of 1kms^{-1} to 2kms^{-1}.

A second aspect is the timing of the pre-ELM structures compared to the radially propagating ELM laments. The radial propagation of ELM laments through the SOL is ob- served after the crash of the pedestal. In the presented observations the footprint structures appear already prior to the ELM crash, during the onset of the ELM.

The nature of the observed propagating structures has similar features to previous observations of strike-line splitting during the application of RMPs; cf. ref. [15]. A requirement for strike-line splitting is a change in the topology of the plasma. This is evidence of a magnetic perturbation

of the plasma edge already in the phase before the ELM crash, e.g. formed by internal modes, additional current laments in the plasma edge, the applied RMP field or a combination of these. The recent findings by Kirket al. [11] have shown lobe structures during RMP phases in the near X-point region on MAST. Such lobes create footprint patterns on the divertor plates similar to RMP experiments in L-mode plasmas. However, unusual for strike-line splitting by static RMPs is the radial propagation of the footprint pattern. This points towards a dynamic nature of the observed structures. It has been reported that additional thermoelectric currents in the plasma edge during the onset of an ELM can lead to the formation of similar footprint patterns [26, 27].

4. INTERPRETATION BASED ON THE THERMOELECTRIC CURRENT MODEL

A loss of particles, preferably electrons, during the inter-ELM phase is seen as the drop in the edge electron temperature. This causes an initial heat pulse transported through short connection length flux tubes [28] to the targets leading to an increase of the electron temperature on the outer target relative to the inner target; cf. Evans et al. [29]. The thermal difference causes an onset of thermoelectric currents between the two targets which than self-amplies and leads to a further change in the magnetic topology as presented in [26, 27]. The loss of mainly electrons will cause an increase in the radial electric field at the edge, damping the electron losses and results in a continued increase of the edge electron temperature while the self-amplication process of the thermoelectric currents could continue.

An application of the thermoelectric current model to a strongly perturbed RMP plasma results in one main difference regarding previous applications which also consider the intrinsic error field as the initial perturbation. This is that the RMPs result in much larger regions of short connection length flux tubes leading to a current density on the target considerably smaller than in the case of intrinsic error fields; here assumed to be $1.5\mathrm{Acm}^{-2}$. Figure 4 shows the prediction of the thermoelectric current model (solid) for the pre-ELM structures compared to the measured heat flux (dashed); for the discharge with JET Pulse Number 83462. The dashed-dotted line gives the expected penetration depth based on the vacuum model only considering the RMP fields.

By comparison of the vacuum modelling to the thermoelectric current model results, the effect of the additional thermoelectric edge current (about 2kA) is seen. The observed pre-ELM structures cannot be explained without considering these additional edge currents that cause a strong change of the magnetic topology.

A further increase of the thermoelectric current results in agreement of the predicted penetration depth (solid) and experimentally observed heat flux prole (dashed) during the ELM crash; see Fig.5. The model is applied analogous to ref. [27] with a thermoelectric edge current of 4.6kA.

DISCUSSION

The thermoelectric current model can predict the appearance of the pre-ELM structures, but not their radial propagation. Considering the work by Harting et al. [15], and the model predicted edge

current increase, the propagation of these structures seems to be understandable as a toroidal shift of existing footprint structures. Based on the following simple considerations, it can be shown that such an explanation is not valid: (1) Additional edge currents cause a decrease of the local q value, (2) this leads to a toroidal shift of the lobe like structures, (3) however, the lobes then shift in such a way that, at a xed toroidal angle, footprints structures appear to shrink. This is opposite to the observations!

A more likely explanation can be found by considering the existence of ballooning modes at that early phase of the ELM, which are enhanced by the RMPs. Simulation results from the reduced MHD code JOREK, have shown that radial propagating stripes in the heat flux on the divertor, are linked to rotating ballooning modes during the ELM [30]. The modelling has stated a dependence of the radial propagation direction on whether the ballooning mode rotation is clockwise or anti-clockwise. The experimentally found radial displacement of the stripes on the divertor corresponds to a lament rotation in the diamagnetic drift direction, which is opposite to the lament rotation that could be induced by the Neutral Beam Injection at JET. A radial propagation of the pre-ELM structures could therefore be due to the RMP effects on the ballooning mode stability, including threshold and growth rate, whereas the mode numbers not necessarily are similar to the dominant RMP mode. Dedicated simulations considering RMPs have not been carried out. However, experiments has shown that an addition of RMPs causes a slowing down of the toroidal plasma rotation. A slower rotation of the ballooning modes leads to a reduction of the radial propagation speed of the structures. This is in-line with the experimentally observed difference in the propagation speed of the pre-ELM structures compared to the ELM stripes, seen without RMPs (see Pamela et al. [30]).

Further studies are needed focusing on the discussed effects and if they can fully explain the experimental observations. Open questions remains in the field of the propagation speed and its link to the poloidal rotation of ballooning modes and the time scale of the self-amplication of the thermoelectric current compared to the time scale of the pre-ELM structures. Furthermore, what is the RMP effect on the radial propagation speed of ELM and inter-ELM laments?

SUMMARY

In this letter we have presented recent observations of pre-ELM structure in the divertor heat loads. This is seen as the appearance of a dynamic heat flux pattern on the divertor plates a few milliseconds before the ELM crash accompanied by a drop in the edge electron temperature and an increase of the D_α emission. A difference in the radial displacement and propagation speed of this pattern has been observed for different q_{95} showing a step between a value of 3.2 and 3.5. The pre-ELM structures appear on a much longer time-scale than known from typical ELM crash rise times. This suggests the inter-ELM phase has an effect on the particle transport to the divertor before the explosive ELM crash. The presented thermoelectric current model explains the appearance of the pre-ELM structures. Its radial propagation can be understood by considering RMP enhanced rotating ballooning modes, as predicted by JOREK code simulations.

ACHNOWLEDGMENTS

Valuable discussions with Peter de Vries and Sebastijan Brezinsek are gratefully acknowledged. M.R. is thankful for the support of Evgenij Bleile and Götz Lehmann. This work, supported by the European Communities under the contract of Association between EURATOM and FZJ, was carried out within the framework of the European Fusion Development Agreement. The views and opinions expressed herein do not necessarily reflect those of the European Commission. Additional support from the Helmholtz Association in frame of the Helmholtz-University Young Investigators Group VH-NG-410 is gratefully acknowledged.

REFERENCES

[1]. F. Wagner etal., Physical Review Letters **49**, 1408 (1982).
[2]. M. Keilhacker etal., Plasma Physics and Controlled Fusion **26**, 49 (1984).
[3]. A. Zhitlukhin etal., Journal of Nuclear Materials **363365**, 301 (2007).
[4]. T. E. Evans etal., Physical Review Letters **92**, 235003 (2004).
[5]. Y. Liang etal., Nuclear Fusion **50**, 025013 (2010).
[6]. W. Suttrop etal., Physical Review Letters **106**, 225004 (2011).
[7]. T. Eich, A. Herrmann, and J. Neuhauser, Physical Review Letters **91**, 195003 (2003).
[8]. M. Jakubowski etal., Journal of Nuclear Materials **415**, S901 (2011).
[9]. S. Devaux etal., Journal of Nuclear Materials **415**, S865 (2011).
[10]. A. Kirk etal., Physical Review Letters **96**, 185001 (2006).
[11]. A. Kirk etal., Physical Review Letters **108**, 255003 (2012).
[12]. M. Jakubowski, S. Abdullaev, K. Finken, and the TEXTOR Team, Nuclear Fusion **44**, S1 (2004).
[13]. T. Evans etal., Journal of Nuclear Materials **363365**, 570 (2007).
[14]. E. Nardon etal., Journal of Nuclear Materials **415**, S914 (2011).
[15]. D. Harting etal., Nuclear Fusion **52**, 054009 (2012).
[16]. V. Philipps, P. Mertens, G. Matthews, and H. Maier, Fusion Engineering and Design **85**, 1581 (2010).
[17]. I. Barlow etal., Fusion Engineering and Design **58-59**, 189 (2001).
[18]. T. Eich etal., Journal of Nuclear Materials **415**, S856 (2011).
[19]. I. Balboa etal., Review of Scientific Instruments **83**, 10D530 (2012).
[20]. S. Devaux etal., 38th EPS Conference on Plasma Physics, O3.108 (2011).
[21]. T. Eich etal., Plasma Physics and Controlled Fusion **47**, 815 (2005), cited by (since 1996) 56
[22]. A. Loarte etal., Plasma Physics and Controlled Fusion **45**, 1549 (2003).
[23]. H.R. Wilson and S.C. Cowley, Physical Review Letters **92**, 175006 (2004).
[24]. A. Kirk etal., Journal of Nuclear Materials **390391**, 727 (2009).
[25]. N.B. Ayed etal., Plasma Physics and Controlled Fusion **51**, 035016 (2009).
[26]. A. Wingen, T.E. Evans, C.J. Lasnier, and K.H. Spatschek, Physical Review Letters **104**, 175001 (2010).

[27]. M. Rack etal., Nuclear Fusion **52**, 074012 (2012).
[28]. A. Wingen, T. Evans, and K. Spatschek, Nucl. Fusion **49**, 055027 (2009).
[29]. T. Evans etal., Journal of Nuclear Materials **390-391**, 789 (2009).
[30]. S. J. P. Pamela etal., Plasma Physics and Controlled Fusion **53**, 054014 (2011)

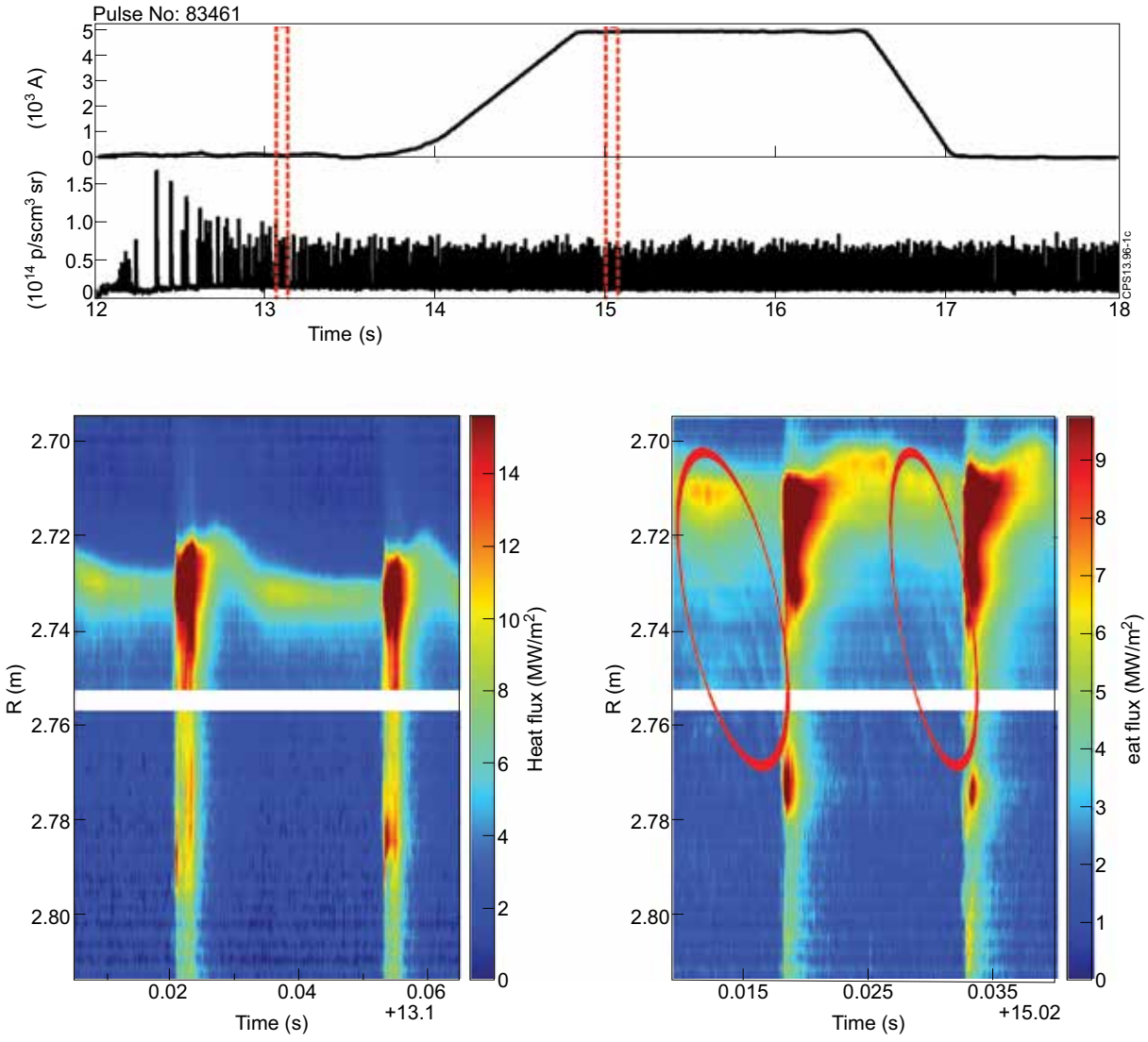

Figure 1: Changes of the divertor heat loads with and without RMPs during the H-mode phase with a plasma current I_p = 1.4MA, a toroidal field B_t = 2.4T, an edge safety factor q_{95} = 4.5. On the top, time-traces of the EFCC amplitude (upper) and the Be II emission from tile 5 (lower), on the bottom, divertor heat loads seen by the infra-red camera without (left) and with (right) RMPs. In the case of the applied RMP field, pre-ELM structures can be observed (region marked by the red ellipses). The white stripe in the heat flux plot indicates the gap between two stacks of the new JET divertor. A reliable measurement of the heat load to the divertor plate is not possible at that positions

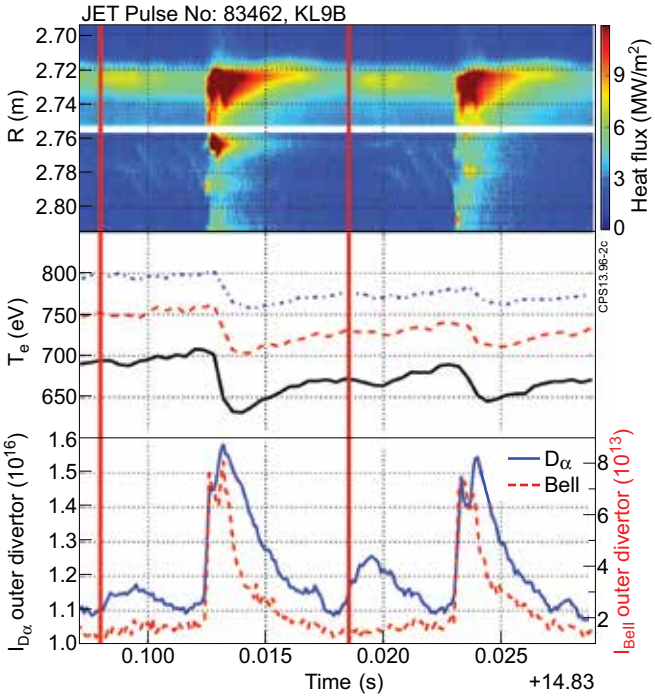

Figure 2: Time-trace of the measured heat load pattern on the outer divertor target tile 5 (top) during the application of RMPs (I_p = 1.4MA, B_t = 1.7T, q_{95} = 3.2). In addition time-traces of the edge electron temperature for different radial positions (middle) and the intensity of the D_α and Be II emission light (bottom) are shown. A drop of the outer edge electron temperature (solid line, R = 3.659m) and an increase of the D_α light intensity can be seen, when the pre-ELM structures are created (red line). The intensity of the Be II light is unaected by the creation of the pre-ELM structure. Edge electron temperatures measured at a more inward position (dashed line, R = 3.640m and dashed-dotted line, R = 3.629m) are less affected than those at the very edge.

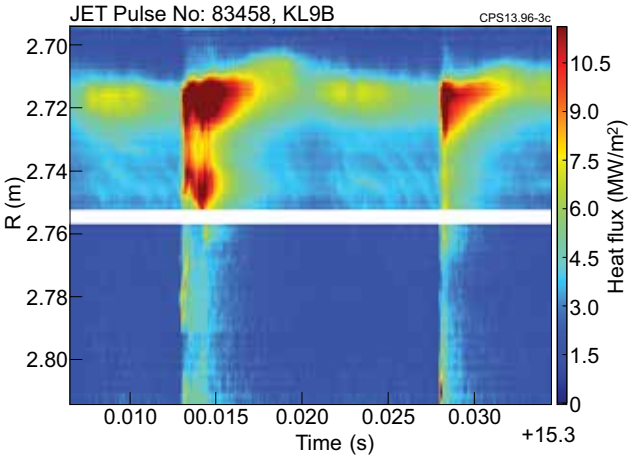

Figure 3: Heat load pattern of the outer divertor (I_p = 1.4MA, B_t = 2.2T, q_{95} = 4.0). The structures propagate with a speed of 7ms^{-1} and are created much closer to the original strike-line compared to the pulse presented in Fig.2 (q_{95} = 3.2).

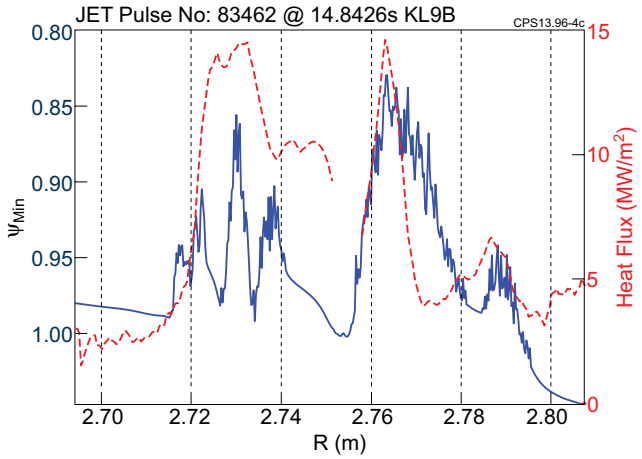

Figure 4: Prediction of the heat flux to the outer target for the pre-ELM structure based on a thermoelectric current model (solid) compared to experiment measurements (dashed). A thermo-electric edge current of 2kA is considered. The dashed-dotted lines gives the predicted penetration depth from the vacuum model as a comparison.

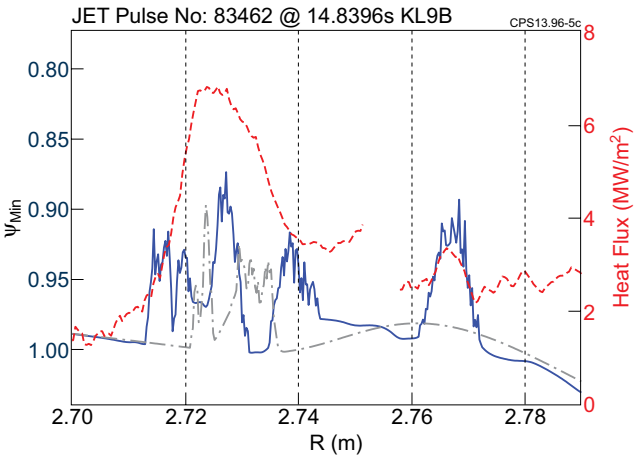

Figure 5: Same as Fig.4 but for the heat flux to the outer target during an ELM crash. The solid line shows the predicted penetration depth and the dashed line gives the measured heat flux profile.